©2008 The Society of Polymer Science, Japan

Polymer Journal

REGULAR ARTICLE

Special Issues –International Symposium on Polymer Crystallization 2007–

Structures of Multilayered Thin Films of Long-Chain Molecules: X-ray Scattering Study

By Ken TANAKA, Kiyoshi ISHIKAWA, Koji NOZAKI,* Naohito URAKAMI, and Takashi YAMAMOTO

The structures of the multilayered thin films of hydrocarbon molecules, which are n-$C_{23}H_{48}$ (C23), n-$C_{25}H_{52}$ (C25), and n-$ClC_{20}H_{40}Cl$ (C20Cl), have been investigated by means of X-ray diffraction. The alternatively layered thin films of two hydrocarbon molecules, the C23/C25/C23/C25/Si, C23/C25/Si, C25/C20Cl/Si, and C20Cl/C25/Si films, were prepared by vacuum evaporation on the Si substrate. The multilayered structural parameters, which are the chain length in each layer, the number of molecule in a layer, the layer thickness, the total film thickness, and the interface structure between different layers are determined from X-ray scattering profiles by using the multilayered model. The obtained parameters are considered to agree with those determined by other techniques. It is concluded that the interface between the different layers of the multilayered films except the C25/C20Cl/Si film are smooth. While in the case of the C25/C20Cl/Si film, the interface structure is disordered. The different deposition sequence leads to difference in interface structure.

KEY WORDS: Thin Film / Multilayered Film / Normal Alkane / X-Ray Diffraction / Interface Structure / Multilayered Structure / Dihalogenoalkane /

In recent years, there have been many studies on organic molecular thin films owning to the fundamental science interest as well as their industrial application including the organic molecular thin film devices. High performance thin film devices are generally composed of a multilayered film. It is unexceptional for the organic molecular thin film devices. The structure of the multilayered film of course affects their physical properties. Therefore, it is important to investigate the multilayered structure, an interface structure in the layer boundary, an interface phenomenon, and so on.

Long hydrocarbon chains are the fundamental frames of many organic molecules, such as lipids, oils, fats, and polymers. Therefore, hydrocarbon plays an important role in structure formation process, such as the crystallizations of fats and polymers, and the formations of lipid membranes. The arrangement of hydrocarbon chains in organic materials affects the physical properties and functions. Therefore, it is very important to elucidate the biomembrane function or industrial application of the materials to understand such an arrangement. Many studies, which aimed at the fundamental understanding of the structure formation of hydrocarbons, have been performed using a simple long hydrocarbon molecule, such as n-alkane. On the basis of condensation of the long hydrocarbon chains, it also became clear that similarity exists in the condensed structure of various systems.[1,2] Long hydrocarbon molecules are arranged in an ordered lamellar structure, in which the molecular chain axes are parallel to each other and their end groups are on the same plane. In a crystal of a long-chain hydrocarbon molecule, the lamellae stack in layers with a three-dimensional (3D) periodicity. On the other hand, the monolayer and bilayer systems are ultrathin films consisting of one lamella and two lamellae, respectively.

A thin film with a long-chain hydrocarbon molecule is often used as a model system for organic thin films. There have been many studies on the structures of the hydrocarbon molecular film prepared by physical vapor deposition methods, such as vacuum evaporation.[3–7] In an evaporated film system with a long chain of hydrocarbon molecules, two typically preferred molecular orientation states were observed. One is the "perpendicular orientation state," in which molecules appear with their chain axes approximately perpendicular to the substrate surface, and the other is the "parallel orientation state," in which molecular chain axes are parallel to the substrate surface.[3–7] Molecular orientation behavior depends on preparation conditions. In a fatty acid[3] and n-alkane evaporated films,[7] the perpendicular orientation state tends to appear when the deposition rate is low or the substrate temperature is high. The dependence of the type of substrate on the molecular orientation was also confirmed. It is important to reveal the mechanism of the formation of the characteristic molecular orientation not only for basic science fields but also for the application of the organic thin film, particularly from the aspect of effective functional generation by controlling the molecular orientation.

Since thin film systems have the large surface area and a large interface area, they often show interesting phenomena, which are peculiar to the thin film system. "Surface freezing" in a long-chain hydrocarbon molecular system is a typical surface phenomenon.[8,9] The characteristic monolayer of n-alkane molecules forms on the bulk liquid surface at temperatures above the bulk melting point, where the molecular chain axes are almost perpendicular to the bulk free surface.[9] The formation of n-alkane the surface monolayer is also observed in ultrathin films of n-alkanes on a solid substrate, such as SiO_2.[10] The perpendicular arrangement of the n-alkane molecules in the

Department of Physics, Graduated School of Science and Engineering, Yamaguchi University, Yamaguchi 753-8512, Japan
*To whom correspondence should be addressed (Tel: +81-83-933-5679, Fax: +81-83-933-5273, E-mail: nozaki@yamaguchi-u.ac.jp).

monolayer on the SiO_2 substrate have been confirmed by various experimental techniques, which are mainly X-ray reflectivity and ellipsometry.[11–19] The existence of the parallel layer, where the molecules lie with their molecular axes parallel to the substrate surface, under the perpendicular monolayer has been discussed. Detail structural analysis in the interface is necessary to elucidate the existence of such parallel layer.

Hydrocarbon molecules are also used in this work as model molecules for various organic molecules, and the multilayered structures of them are studied by means of X-ray diffraction. When the multilayered structure is investigated, the techniques established for the inorganic thin film devices are usually used. They are, for example, X-ray photoelectron spectroscopy (XPS), secondary ion mass spectroscopy (SIMS), electron microscope (SEM, TEM), ellipsometry, X-ray reflectivity measurement, etc. However, some of them are not available for organic substance. Because organic materials consist of a few kinds of light elements such as C, H, N, O, micronutrient analysis technique is not available, and the substance is easily damaged by high power electron beams and ion beams. Many studies[20–24] used the X-ray reflectivity measurement[25,26] for the estimation of the film thickness and the evaluation of the interface roughness of the organic thin films. However, the signal of the X-ray reflectivity is too weak to determine the multilayered structure due to the small difference in density between the individual layers in the case of the organic multilayered film. Recently, some works[27–31] have performed the atomic scale structural characterization of thin films by procedure SuPREX[32,33] for the quantitative structural refinement using X-ray diffraction profiles. This method is originally developed for inorganic multilayer films, and it is difficult to use for the thin film of the organic molecules which consist of many atoms and have complex molecular structure. Since the X-ray scattering intensity is relatively low in the case of the organic thin film, it is difficult to analyze the atomic scale structure, although the atomic arrangement in the individual layers of the organic thin film was tried to be determined by this special method.[27]

In this work, we focus on the multilayered structure of the organic thin film. Normal alkanes (n-C_nH_{2n+2}: abbreviated as Cn) and n-α,ω-dihalogenoalkanes (n-$C_nH_{2n}X_2$: abbreviated as CnX) are selected as model organic molecules. Alternatively multilayered film of two model molecules are prepared by vacuum evaporation, where the lamellar surface of each layer is parallel to substrate (in the perpendicular orientation state) shown in Figure 1. The multilayered structural aspects, which are the layer thicknesses, the molecular arrangements in individual layers, the interface roughness, etc., are tired to be determined by comparing the observed X-ray scattering profile of the alternative multilayered film with the calculated profiles from the multilayered model defined in the next section.

MULTILAYERED MODEL

Figure 2(a) shows the multilayered model proposed in order to obtain the structural aspects of multilayered film from X-ray scattering profiles. The molecules are in the perpendicular orientation state in each layer. The two kinds of layers, the A and B layers, consisting of different hydrocarbon molecules alternatively stack; the periodic molecular array in each layer is reproduced in this model. The n_A and n_B are the number of the molecules, the L_A and L_B are the molecular lengths along the normal direction to the layer surface, and the d_A and d_B are the gaps between the molecules along the surface normal, in the A and B layers, respectively. Thus, the thicknesses of the A and B layers are obtained as

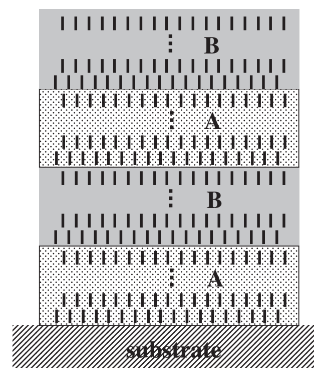

Figure 1. Alternatively multilayered film of two model molecules. In each layer the lamellar surface layer is parallel to the substrate surface, where the film is in the perpendicular orientation state.

$$n_A(L_A + d_A) \text{ and } n_B(L_B + d_B), \tag{1}$$

respectively. In present case, since the X-ray scattering profiles used here are along the surface normal direction in reciprocal space, the 1-dimensional (1D) electron density along the surface normal $\rho(z)$ contributes to the scattering intensity, where the surface normal direction is defined as z direction here. Figure 2(b) shows the 1D electron density distribution along the surface normal used here. It is difficult to obtain the structure details due to poor intensity and poor resolution of the observed X-ray diffraction profile. The undulation of the electron density due to the individual carbon atom arrangement along one hydrocarbon chain is approximately smoothed evenly to ρ_{cA} or ρ_{cB} in this model. While in the gap region between the molecules, the electron densities are assumed to be ρ_{aA} and ρ_{aB}, respectively. Thus, the scattering amplitude is given by

$$A(S_z) = \int_{\text{film}} \rho(z) e^{2\pi i z S_z} dz, \tag{2}$$

where S_z is a scattering vector along the surface normal direction.

On the assumption that the interface between the different layers is enough smooth to make the scattering X-rays coherent over the multilayered film, the scattering intensity from this multilayered model can be calculated by

$$I(S_z) \propto |A(S_z)|^2. \tag{3}$$

For the multilayered film of $N_{\text{total}} = 2N_s$ layers, the total scattering intensity $I(S_z)$ is calculated as

 ©2008 The Society of Polymer Science, Japan

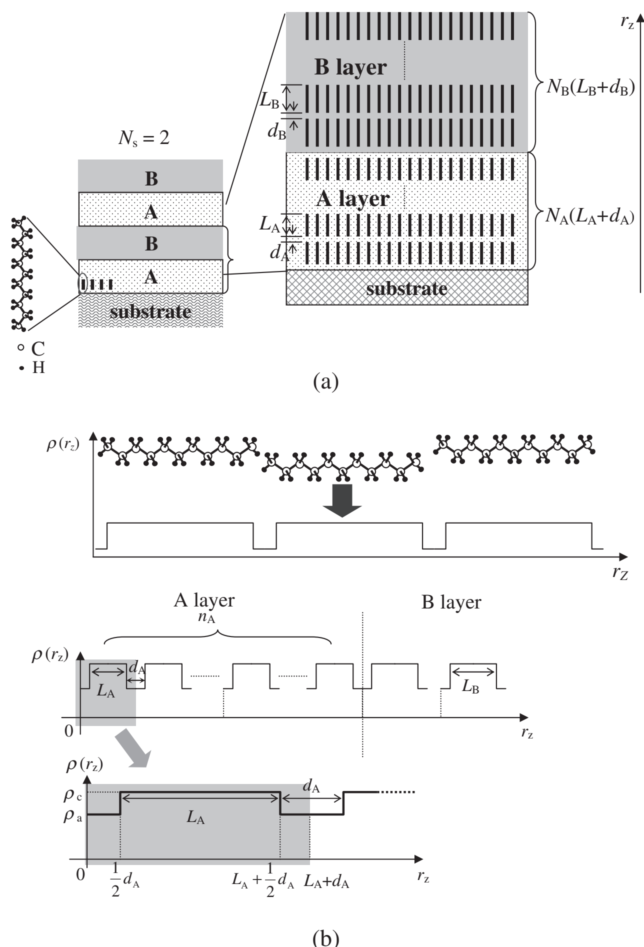

Figure 2. Multilayered model proposed in order to estimate the structural aspects of multilayered film from X-ray scattering profiles (a), and 1D electron density distribution along the surface normal used in the multilayered model (b). The n_A and n_B are the number of the molecules, the L_A and L_B are the molecular lengths along the normal direction to the layer surface, and the d_A and d_B are the gaps between the molecules along the surface normal, in the A and B layers, respectively. The undulation of the electron density due to the individual carbon atom arrangement is approximately smoothed evenly to ρ_{cA} or ρ_{cB} in this model. While in the gap region between the molecules, the electron densities are assumed to be ρ_{aA} and ρ_{aB}, respectively.

$$
\begin{aligned}
I(s_z) = LP \cdot Sc \cdot D \cdot \frac{\sin^2 N_s \pi S_z L_s}{\sin^2 \pi S_z L_s} \\
\times \left[\frac{1}{\pi^2 S_z{}^2} A'_{\rm mol}{}^2 \frac{\sin^2 n_A \pi S_z (L_A + d_A)}{\sin^2 \pi S_z (L_A + d_A)} \right. \\
+ \frac{1}{\pi^2 S_z{}^2} B'_{\rm mol}{}^2 \frac{\sin^2 n_B \pi S_z (L_B + d_B)}{\sin^2 \pi S_z (L_B + d_B)} \\
+ \frac{2}{\pi^2 S_z{}^2} A'_{\rm mol} B'_{\rm mol} \cos \pi S_z L_s \\
\left. \times \frac{\sin n_A \pi S_z (L_A + d_A)}{\sin \pi S_z (L_A + d_A)} \frac{\sin n_B \pi S_z (L_B + d_B)}{\sin \pi S_z (L_B + d_B)} \right], \quad (4)
\end{aligned}
$$

where

$$L_s = n_A(L_A + d_A) + n_B(L_B + d_B), \quad (5)$$

$$
\begin{aligned}
A'_{\rm mol} &= (\rho_{cA} - \rho_{aA}) \sin \pi S_z L_A + \rho_{aA} \sin \pi S_z (L_A + d_A), \\
B'_{\rm mol} &= (\rho_{cB} - \rho_{aB}) \sin \pi S_z L_B + \rho_{aB} \sin \pi S_z (L_B + d_B), \quad (6)
\end{aligned}
$$

$$D = \exp(-S_z{}^2 \langle u_z{}^2 \rangle), \quad (7)$$

LP is the Lorentz-Polarization factor, and S_c is the scale factor (see APPENDIX). D is Debye-Waller factor, and $\langle u_z{}^2 \rangle$ is the mean-square displacement of the molecules along the z direction.

EXPERIMENTAL

Two *n*-alkanes, *n*-tricosane (C23) and *n*-pentacosane (C25), used in this work were purchased from Tokyo Kasei Kogyo. The purities were higher than 98%, and no further purification was carried out. Normal 1,20-dichloroeicosane (C20Cl), which was synthesized by the reduction and chlorination from 1,20-eicosanedionic acid.[34]

Alternatively multilayered films of the two hydrocarbon molecules were prepared by vacuum evaporation on Si (100) substrates using a standard vacuum evaporation apparatus (ULVAC, PVC160). The Si wafer was cut into the suitable size pieces ($18 \times 18\,\text{mm}^2$, 0.37 mm in thickness) for substrates. The Si substrates were washed by toluene and were mounted on a metal block susceptor without any surface treatments. The substrate temperature was kept at room temperature (about 27 °C) during the deposition.

Two source materials were independently evaporated from two tungsten boats. The evaporation rates of the two sources were individually regulated by controlling the evaporation temperatures. A K-type thermocouple was attached to the boat, and the temperature of the boats were regulated within ±0.5 °C by controlling the electric current directly passing through them using PID type temperature controller (SHIMADEN, SR52). Vacuum evaporation was performed at a pressure of 2.0×10^{-3} Pa. The evaporation rates and film thickness were monitored using a standard deposition monitor (ULVAC, CRTM-6000) with a quartz crystal oscillator during deposition process. Figure 3 shows a typical deposition sequence of the alternatively multilayered film. First the A material was deposited on the substrate. After a certain deposition period, the evaporation of the A material was stopped. Successively, the deposition of the B material on the A layer was started. Thus, the A and B materials were alternatively deposited.

X-Ray scattering profiles of the multilayered films were collected by using two types of diffractometers. One was a high-resolution type diffcartometer (Rigaku, TTR-III) with a two-crystals Ge (220) monochrometer. This high-resolution type diffractometer was only used for C23/C25 multilayered films. The other is a standard type diffractometer (Rigaku, RAD-IIA) with a graphite (0002) monochrometer. In both types, symmetrical reflection geometry with Cu-Kα radiation was used, where the sample film with substrate was attached to a sample holder in parallel, so that only the X-ray reflections at the scattering vectors perpendicular to the substrate surface, were observable. The conditions of the X-ray diffraction are listed in Table I.

©2008 The Society of Polymer Science, Japan

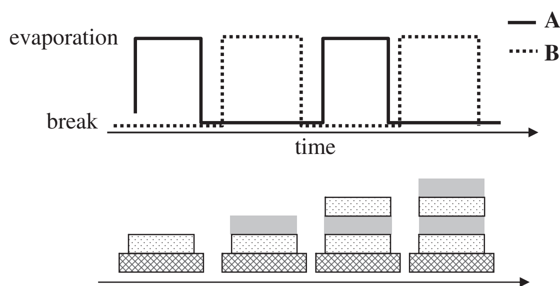

Figure 3. Typical deposition sequence of the alternatively multilayered film.

Table I. X-Ray diffraction conditions

high-resolution type	
diffractometer	Rigaku, TTR-III
source power	50 kV–300 mA
X-ray	Cu-Kα
scan method	θ–2θ, step scan
$\Delta 2\theta$	0.01°
2θ range	1°–30°
fixed time	1 s
slit	DS: 0.05 mm, SS: 0.2 mm, RS 0.2 mm
standard type	
diffractometer	Rigaku, RAD-IIA
source power	35 kV–20 mA
X-ray	Cu-Kα
scan method	θ–2θ, step scan
$\Delta 2\theta$	0.02°
2θ range	1°–30°
fixed time	1 s
slit	DS: 0.5°, SS: 0.5°, RS 0.15 mm

The surface morphology of the evaporated film was observed by using scanning probe microscope (SPM; SII Nanotechnology, SPI3800N). The dynamic force mode (DFM) was used with a DFM cantilever (15 N/m, 120 kHz). The scanning area was $10 \times 10\,\mu m^2$, and the scanning rate was 0.5 Hz.

RESULTS AND DISCUSSION

Figure 4(a)–4(c) show X-ray scattering profiles of the C23/C25/C23/C25/Si four layered, C25/Si, and C23/Si films, respectively. In the profiles of the C25/Si and C23/Si films (Figure 4(b) and 4(c)), all observed peaks are the 00*l* Bragg peaks from the molecular lamellar stacking; the molecules in these films are arranged in lamellar structure similar in a bulk crystalline state. This result also indicates that the (00*l*) planes are parallel to the film surface; the film is in the perpendicular orientation state. It was found that the profile of the four layered film (Figure 4(a)) cannot be composed by a simple combination of the C25/Si and C23/Si profiles, but some extra peaks are observed. These peaks are expected to be a result of the interference of the X-rays scattering from the different layers, what we call the "interlayer coherency" of X-rays.

In order to confirm the interlayer coherency, the X-ray scattering intensity was calculated from the multilayered model

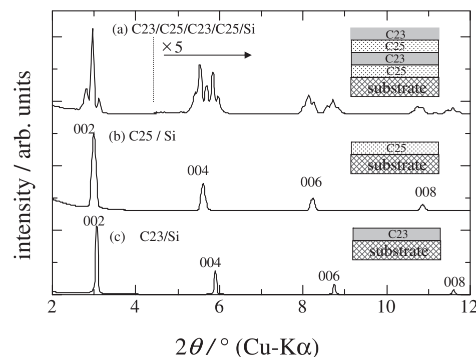

Figure 4. X-Ray scattering profiles, (a): of the C23/C25/C23/C25/Si four layered film, (b): of the C25/Si monolayer film, and (c): of the C23/Si monolayer film, respectively. All profiles were collected by the standard resolution type diffractometer.

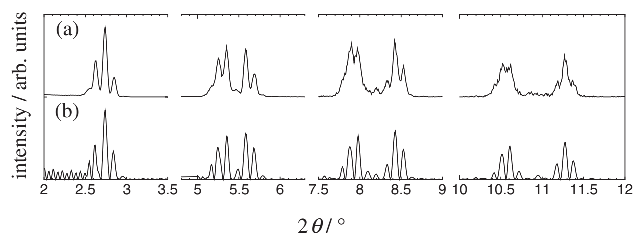

Figure 5. Observed (a) and calculated (b) high-resolution X-ray scattering profiles of C23/25/C23/C25/Si four layered film. The sample is different from that for Figure 4(a).

by formula (4), where the interlayer coherency is included. The structural parameters were also optimized by comparing the calculated and observed profiles by means of least square method with simulated annealing algorithm. The initial 1D electron density parameters, $\rho_{cC23} = 57\,e/\mathrm{nm}$, $\rho_{cC25} = 57\,e/\mathrm{nm}$, $\rho_{aC23} = 10\,e/\mathrm{nm}$, $\rho_{aC25} = 10\,e/\mathrm{nm}$, $d_{C23} = d_{C25} = 0.18$ nm, and $d_{C20Cl} = 0.10\,\mathrm{nm}$ are used.[35,36] Figure 5 shows the observed and calculated high-resolution X-ray scattering profiles of a C23/25/C23/C25/Si four layered film. The both profiles show a good agreement, although the difference in the fine structure remains due to poor resolution of the observed profile. Thus, the existence of the interlayer coherency is confirmed. Figure 6(a) and 6(b) show the SPM (DFM) images of the surface of the C23/Si film. In Figure 6(a), the stacked flat terraces are observed. In the cross sectional image in Figure 6(b), the surface is flat over relatively wide area ($1000 \times 1000\,\mathrm{nm}^2$), and only a few steps are observed. The average step height of them corresponds to one molecular length of an all-trans C23 molecule. From the flat morphology of the C23/Si film surface, it is easily expected that the layer interface of the C23-C25 multilayered thin film is smooth enough for the interlayer coherency.

Thus, some of the multilayered structural parameters were obtained for a few C23/C25/C23/C25/Si films prepared by different conditions and are listed in Tables II, where the high-resolution X-ray scattering profiles were used. Total film thicknesses measured by using SPM are also listed. The other parameters not listed in Table II were fixed at the suitable

 ©2008 The Society of Polymer Science, Japan

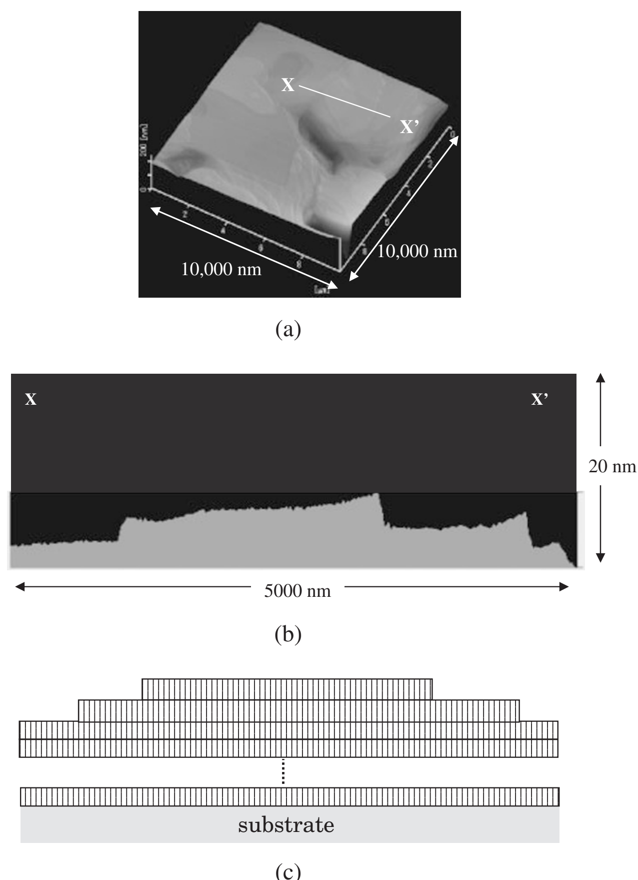

Figure 6. (a): SPM (DFM) surface image of the C23/Si film, (b): the cross sectional image along the X-X′ line in the surface image, and (c): the schematics of the cross section of the C23/Si film.

Table II. Structural parameters of C23/C25/C23/C25/Si (4 layered) films determined from the high-resolution X-ray scattering profiles

$L_{C23} + d_{C23}$ [nm]	$L_{C25} + d_{C25}$ [nm]	N_{C23}	N_{C25}	total film thickness [nm] (calculation)	(SPM)
3.14	3.34	2	7	58	40
3.15	3.36	8	16	158	130
3.13	3.38	25	28	345	310
3.16	3.38	25	35	394	370

initial values or were varied within the narrow limits around the initial values during the calculation. The chain lengths obtained for C23/C25/C23/C25/Si films are almost same as those of bulk crystals.[1] Total film thicknesses obtained by the optimization of the model approximately agree with those measured by using SPM. Since the film thickness obtained by SPM is not the average value but that at a local area in the sample film, it is allowed for a certain level of difference between the thicknesses obtained by the simulated annealing and using SPM.

Figure 7(a)–(c) show the observed and calculated X-ray scattering profiles of the C25/C23/Si, C20Cl/C25/Si, and C25/C20Cl/Si two layered films, respectively. It is clear that these films are also in the perpendicular orientation state like C23/C25/C23/C25/Si four layered film. It seems that the scattering intensity which results from the interference between

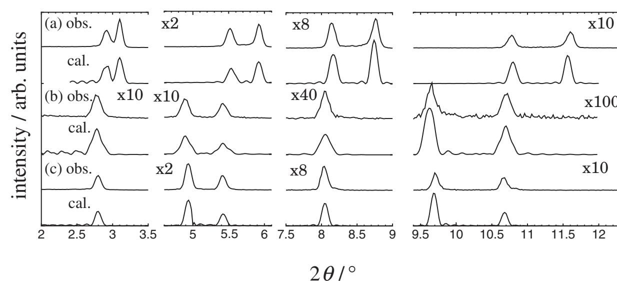

Figure 7. The observed and calculated standard resolution X-ray scattering intensities of the (a): C23/C25/Si, (b): C20Cl/C25/Si, and (c): C25/C20Cl/Si two layered films.

the different layers is weak in the observed profiles. Hence, in the case of the two layered film ($N_s = 1$), the interference factor I_s is multiplied into the cross term of the scattering intensity in the multilayered model to evaluate a magnitude of the interlayer coherency. For $N_s = 1$, the intensity in formula (4) is modified as

$$\begin{aligned} I(s_z) &= LP \cdot Sc \cdot D \\ &\times \left[\frac{1}{\pi^2 S_z{}^2} A'_{\text{mol}}{}^2 \frac{\sin^2 n_A \pi S_z (L_A + d_A)}{\sin^2 \pi S_z (L_A + d_A)} \right. \\ &+ \frac{1}{\pi^2 S_z{}^2} B'_{\text{mol}}{}^2 \frac{\sin^2 n_B \pi S_z (L_B + d_B)}{\sin^2 \pi S_z (L_B + d_B)} \\ &+ I_f \frac{2}{\pi^2 S_z{}^2} A'_{\text{mol}} B'_{\text{mol}} \cos \pi S_z L_s \\ &\left. \times \frac{\sin n_A \pi S_z (L_A + d_A)}{\sin \pi S_z (L_A + d_A)} \frac{\sin n_B \pi S_z (L_B + d_B)}{\sin \pi S_z (L_B + d_B)} \right]. \end{aligned} \quad (8)$$

When the system have complete interlayer coherency, the interference factor I_f takes a value of 1. On the other hand, when the interlayer coherency is weaker in the multilayered film system, the I_f decreases to 0. The interlayer coherency is considered to be affected by the interface structure. When the interface has smooth structure, where the molecules of the upper layer stack with keeping the translational lattice symmetry in the lower layer, the high interlayer coherency is expected. On the other hand, when there are vacancies and some kinds of defects (for example, a lying molecule) at layer interface, and the translational symmetry is not maintained any longer at relatively rough interface, the interlayer coherency may be weak.

The multilayered structural parameters as well as the interference factors determined for some C23/C25/Si, C20Cl/C25/Si, and C25/C20Cl/Si films prepared by different conditions are listed in Tables III, IV, and V, respectively. In these determinations, standard resolution X-ray scattering profiles were used. The chain length of about 1.5 nm obtained for C20Cl is shorter than that predicted from all trans hydrocarbon chain. In bulk crystal of C16Cl, the molecular chains tilt from the lamellar surface normal.[36] Therefore, it is expected that the C20Cl chains in the thin film also tilt from the surface normal. Since the L_{C20Cl} is a length along the layer surface normal, the value of 1.5 nm approximately corresponds to that obtained according to the assumption that the C20Cl

©2008 The Society of Polymer Science, Japan

Table III. Structural parameters of C23/C25/Si (2 layered) films determined from the high-resolution X-ray scattering profiles

$L_{C23} + d_{C23}$ [nm]	$L_{C25} + d_{C25}$ [nm]	N_{C23}	N_{C25}	total film thickness [nm] (calculation)	(SPM)	I_f
3.15	3.36	11	11	73	45	0.49
3.17	3.40	16	16	106	60	0.66
3.14	3.35	19	23	136	140	0.25*

*The observed and calculated X-ray scattering profiles are shown in Figure 7(a).

Table IV. Structural parameters of C20Cl/C25/Si film determined from the standard resolution X-ray scattering profiles

L_{C20Cl} [nm]	L_{C25} [nm]	N_{C20Cl}	N_{C25}	total film thickness [nm] (calculation)	(SPM)	I_f
1.95	3.36	6	7	35	40	0.14
1.89	3.38	13	14	72	100	0.61
1.87	3.32	25	13	90	150	0.62*
1.86	3.38	35	20	133	240	0.35
1.87	3.37	45	24	165	130	0.40

*The observed and calculated X-ray scattering profiles are shown in Figure 7(b).

Table V. Structural parameters of C25/C20Cl/Si film determined from the standard resolution X-ray scattering profiles

L_{C25} [nm]	L_{C20Cl} [nm]	N_{C25}	N_{C20Cl}	total film thickness [nm] (calculation)	(SPM)	I_f
3.40	1.90	12	16	71	71	0.063
3.36	1.87	13	22	85	100	0.048
3.35	1.86	16	30	110	110	0.014
3.37	1.86	23	40	152	240	0.082*
3.38	1.87	29	58	206	250	0.044

*The observed and calculated X-ray scattering profiles are shown in Figure 7(c).

chains in the thin film have same tilt angle as bulk crystal. (In the strict sense, the address term "the perpendicular orientation state" may be inappropriate, because the molecular chain axes are not perpendicular to the substrate. However, we call here the state in which the lamellar surface is parallel to the substrate surface "the perpendicular orientation state.")

Figure 8 shows layer thickness dependence of the interference factor I_f of the C23/C25/Si, C20Cl/C25/Si, and C25/C20Cl layered films. It is interesting to note that all interference factors of the C25/C20Cl/Si films are smaller than those of the C20Cl/C25/Si and C23/C25/Si films. (The small I_f value obtained for the thinnest C20Cl/C25/Si film sample is considered to be caused by poor X-ray scattering intensity.) When the C25 layer is first deposited on the substrate, the film exhibits high interlayer coherency. This result closely relates to the interface structure. It is expected that the interface of the C20Cl/C25/Si film is smoother than that of the C25/C20Cl/Si film. Figure 9(a) and 9(b) show SPM (DFM) images of the surface of the C20Cl/Si film. As compared to the C23/Si film, the surface of the C20Cl film shows rough morphology. When the upper C25 layer stacks on the lower C20Cl layer, the disordered interface is formed due to the rough surface of the lower C20Cl layer. Therefore, the interference factor is small in the case of C25/C20Cl/Si film. While, in the case of C20Cl/C25/Si film, since the base C25 surface is considered to be relatively flat similar to the C23 surface, the ordered interface is formed. The smooth interface leads to high interface coherency. Thus, it becomes clear that the different preparation sequence results in the different interface structure in the C20Cl-C25 bilayer thin film system.

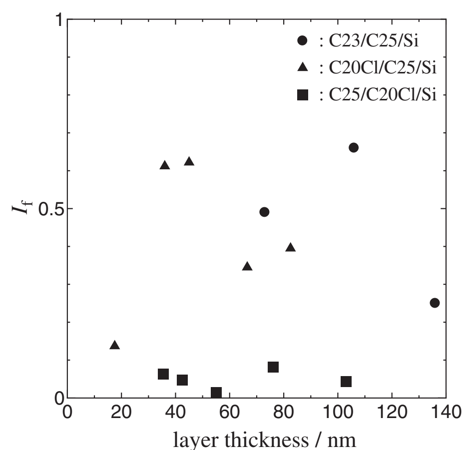

Figure 8. Layer thickness dependence of the interference factor I_f of the C23/C25/Si (circles), C20Cl/C25/Si (triangles), and C25/C20Cl/Si two layered (squares) films.

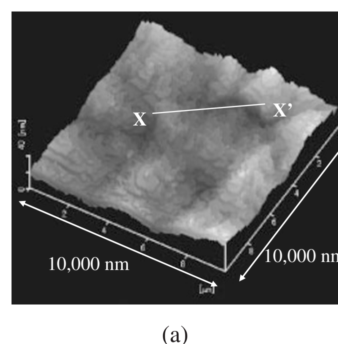

(a)

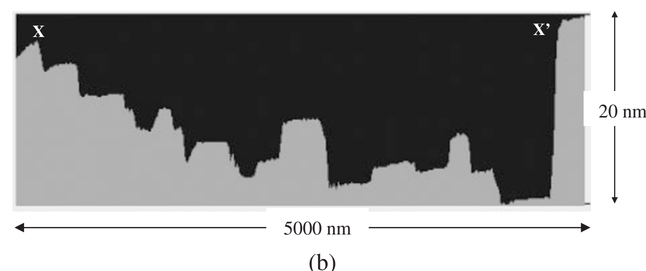

(b)

Figure 9. SPM (DFM) surface image (a) and the cross section image (b) along the X-X′ line in the surface image of the C20Cl/Si film. The surface morphology is relatively rough, when it is compared with that of the C23/Si film.

CONCLUSION

We have investigated the multilayered structure of the alternatively layered thin films of two hydrocarbon molecules by using X-ray scattering profiles. The major results are summarized as follows.

©2008 The Society of Polymer Science, Japan

The molecular lengths and the number of the molecule in each layer were estimated from the X-ray scattering profiles by using the multilayered model. The molecular lengths obtained here are suitable values, which are similar to the molecular lengths in bulk crystals. The total film thicknesses obtained from the X-ray scattering profiles approximately correspond to those measured by using SPM. Furthermore, it becomes clear that the interface is smooth enough for interface coherency for the C23-C25 layered thin film system. With regards to the C20Cl/C25/Si and C25/C20Cl/Si thin films, the interface structure depends on the preparation sequence. When the C25 is deposited on the Si substrate first and the C20Cl is successively deposited on the base C25 layer, the smooth interface is formed, resulting in the high interface coherency. On the other hand, in the case of the C25/C20Cl/Si, the disordered interface is formed, resulting in the absence of the interface coherency.

Acknowledgment. The authors are very grateful to Professor Yoshihiro Ogawa, for sample preparation. The authors express their thanks to Dr. Hiromi Ota and Mr. Yuzuru Maki at Rigaku Corporation for their assistance of collection of X-ray scattering profiles. This work was supported by a Grant-Aid for Scientific Research (No. 14540378) from the Ministry of Education, Culture, Sports, Science, and Technology.

Appendix

X-Ray Scattering Intensity from the Multilayered Model

With regards to the multilayered model in Figure 2, the scattering amplitudes for one molecule in the A and B layers, A_{mol} and B_{mol}, *i.e.*, structure factors of one molecule are

$$\begin{aligned} A_{\mathrm{mol}}(S_z) &= \int_0^{L_A+d_A} \rho(z)\exp(2\pi S_z z)dz \\ &= \frac{1}{\pi S_z}\exp\{\pi i S_z(L_A+d_A)\}A'_{\mathrm{mol}} \\ B_{\mathrm{mol}}(S_z) &= \frac{1}{\pi S_z}\exp\{\pi i S_z(L_B+d_B)\}B'_{\mathrm{mol}}, \end{aligned} \qquad (A{\cdot}1)$$

where,

$$\begin{aligned} A'_{\mathrm{mol}} &= (\rho_{cA}-\rho_{aA})\sin\pi S_z L_A + \rho_{aA}\sin\pi S_z(L_A+d_A) \\ B'_{\mathrm{mol}} &= (\rho_{cB}-\rho_{aB})\sin\pi S_z L_B + \rho_{aB}\sin\pi S_z(L_B+d_B). \end{aligned} \qquad (A{\cdot}2)$$

The scattering amplitudes for the A and B layers, A_{unit} and B_{unit}, are derived as

$$\begin{aligned} A_{\mathrm{unit}} &= \sum_{j=0}^{n_A-1}\exp\{2\pi i S_z j(L_A+d_A)\}A_{\mathrm{mol}}(S_z) \\ B_{\mathrm{unit}} &= \sum_{j=0}^{n_B-1}\exp\{2\pi i S_z j(L_B+d_B)\}B_{\mathrm{mol}}(S_z). \end{aligned} \qquad (A{\cdot}3)$$

When $N_s = 1$ (in the case of B/A/substrate film), the total scattering intensity is given by

$$\begin{aligned} I(S_z) &= C_0|A_{\mathrm{unit}}+B_{\mathrm{unit}}|^2 \\ &= C_0\left[\frac{1}{\pi^2 S_z^2}{A'_{\mathrm{mol}}}^2\frac{\sin^2 n_A\pi S_z(L_A+d_A)}{\sin^2\pi S_z(L_A+d_A)} + \frac{1}{\pi^2 S_z^2}{B'_{\mathrm{mol}}}^2\frac{\sin^2 n_B\pi S_z(L_B+d_B)}{\sin^2\pi S_z(L_B+d_B)} + \frac{2}{\pi^2 S_z^2}A'_{\mathrm{mol}}B'_{\mathrm{mol}}\cos\pi S_z L_s \times \frac{\sin n_A\pi S_z(L_A+d_A)}{\sin\pi S_z(L_A+d_A)}\frac{\sin n_B\pi S_z(L_B+d_B)}{\sin\pi S_z(L_B+d_B)}\right], \end{aligned} \qquad (A{\cdot}4)$$

where,

$$C_0 = LP\cdot Sc\cdot D \qquad (A{\cdot}5)$$

and

$$L_s = n_A(L_A+d_A)+n_B(L_B+d_B). \qquad (A{\cdot}6)$$

LP is the Lorentz-Polarization factor, and S_c is the scale factor. The factor D is Debye-Waller factor.

Finally, when $N_s \neq 1$, the Laue factor is multiplied to the formula (A·4),

$$\begin{aligned} I(s_z) &= LP\cdot Sc\cdot D\cdot\frac{\sin^2 N_s\pi S_z L_s}{\sin^2\pi S_z L_s} \\ &\times\left[\frac{1}{\pi^2 S_z^2}{A'_{\mathrm{mol}}}^2\frac{\sin^2 n_A\pi S_z(L_A+d_A)}{\sin^2\pi S_z(L_A+d_A)} + \frac{1}{\pi^2 S_z^2}{B'_{\mathrm{mol}}}^2\frac{\sin^2 n_B\pi S_z(L_B+d_B)}{\sin^2\pi S_z(L_B+d_B)} + I_f\frac{2}{\pi^2 S_z^2}A'_{\mathrm{mol}}B'_{\mathrm{mol}}\cos\pi S_z L_s \times\frac{\sin n_A\pi S_z(L_A+d_A)}{\sin\pi S_z(L_A+d_A)}\frac{\sin n_B\pi S_z(L_B+d_B)}{\sin\pi S_z(L_B+d_B)}\right]. \end{aligned} \qquad (A{\cdot}7)$$

The formula (A·7) indicates the calculated scattering intensity from the multilayered model.

Received: December 5, 2007
Accepted: July 1, 2008
Published: August 12, 2008

REFERENCES

1. B. M. Cravem, Y. Lange, G. G. Shipley, and J. Steiner, in "Handbook of Lipid Research," D. M. Small, Ed., Plenum, New York, 1986, vol. 4.
2. E. B. Sirota, *Langmuir*, **13**, 3849 (1997).
3. K. Sato, H. Takiguchi, S. Ueno, J. Yano, and K. Yase, in "Advances in the Understanding of Crystal Growth Mechanisms," T. Nishinaga, K. Nishioka, J. Harada, A. Sasaki, and H. Takei, Ed., Elsevier Science, Amsterdam, 1997, p349.
4. K. Ueda and M. Ashida, *J. Electron Micros.*, **29**, 38 (1980).
5. K. Fukao, T. Horiuchi, and K. Matsushige, *Thin Solid Films*, **171**, 359 (1989).
6. K. Fukao, *Thin Solid Films*, **197**, 157 (1991).
7. K. Nozaki, R. Saihara, K. Ishikawa, and T. Yamamoto, *Jpn. J. Appl. Phys.*, **46**, 761 (2007).
8. J. C. Earnshaw and C. J. Hughes, *Phys. Rev. A*, **46**, R4494 (1992).
9. X. Z. Wu, E. B. Sirota, S. K. Shinha, B. M. Ocko, and M. Deutsch, *Phys. Rev. Lett.*, **70**, 958 (1993).

©2008 The Society of Polymer Science, Japan

10. C. Merkl, T. Pfohl, and H. Reigler, *Phys. Rev. Lett.*, **79**, 4625 (1997).
11. A. Holtzwarth, S. Leporatti, and H. Riegler, *Europhys. Lett.*, **52**, 623 (2000).
12. H. Schollmeyer, B. Ocko, and H. Riegler, *Langmuir*, **18**, 4351 (2002).
13. H. Schollmeyer, B. Struth, and H. Riegler, *Langmuir*, **19**, 5042 (2003).
14. P. Lazar, H. Schollmeyer, and H. Riegler, *Phys. Rev. Lett.*, **94**, 116101 (2005).
15. U. G. Volkmann, M. Pino, L. A. Altamirano, H. Taub, and F. Y. Hansen, *J. Chem. Phys.*, **116**, 2107 (2002).
16. H. Mo, H. Taub, U. G. Volkmann, M. Pino, S. N. Ehrlich, F. Y. Hansen, E. Lu, and P. Miceli, *Chem. Phys. Lett.*, **377**, 99 (2003).
17. H. Mo, S. Trogisch, H. Tab, S. N. Ehrlich, U. G. Volkmann, F. Y. Hansen, and M. Pino, *Phys. Status Solidi A*, **201**, 2375 (2004).
18. Mo, S. Trogisch, H. Tab, S. N. Ehrlich, U. G. Volkmann, F. Y. Hansen, and M. Pino, *J. Phys.: Condens. Matter*, **16**, S2905 (2004).
19. F. Kruchten, K. Knorr, U. G. Volkmann, H. Taub, F. Y. Hansen, B. Matthies, and K. W. Herwig, *Langmuir*, **21**, 7507 (2005).
20. T. P. Russell, *Mater. Sci. Rep.*, **5**, 171 (1990).
21. M. Stamm, *Adv. Polym. Sci.*, **100**, 358 (1992).
22. M. F. Toney and C. J. Tompson, *J. Chem. Phys.*, **92**, 3781 (1990).
23. T. Miyazaki, A. Shimazu, T. Matsushita, and K. Ikeda, *J. Appl. Plom. Sci.*, **78**, 1812 (2000).
24. T. Miyazaki, A. Shimizu, and K. Ikeda, *Polymer*, **41**, 8167 (2000).
25. L. G. Parratt, *Phys. Rev.*, **95**, 359 (1954).
26. L. Nevot and P. Croce, *Rev. Phys. Appl.*, **15**, 761 (1980).
27. C. W. Miller, A. Sharoni, G. Liu, C. N. Colesniuc, B. Fruhberger, and Ivan K. Schuller, *Phys. Rev. B*, **72**, 104113 (2005).
28. I. K. Schuller, S. Kim, and C. Leighton, *J. Magn. Magn. Mater.*, **200**, 571 (1999).
29. D. Neerinck, H. Vanderstraeten, L. Stockman, J.-P. Locquet, Y. Bruynseraede, and I. K. Schuller, *J. Phys.: Condens. Matter*, **2**, 4111 (1990).
30. J. Guimpel, E. E. Fullerton, O. Nakamura, and I. K. Schuller, *J. Phys.: Condens. Matter*, **5**, A383 (1993).
31. I. K. Schuller and Y. Bruynseraede, *Nanostruct. Mater.*, **1**, 387 (1992).
32. I. K. Schuller, *Phys. Rev. Lett.*, **44**, 1597 (1980).
33. SuPREX is a free software package that can be obtained from a site: ischuller.ucsd.edu.
34. Y. Ogawa and T. Maeno, *Polym. Prepr., Jpn.*, **55**, 750 (2006).
35. G. Strobl, B. Ewen, E. W. Foscher, and W. Piesczek, *J. Chem. Phys.*, **61**, 5257 (1974).
36. N. Nakamura and H. Shimizu, *Acta Crystallogr.*, **E60**, 131 (2004).

 ©2008 The Society of Polymer Science, Japan